



**HAL**  
open science

# Hydrogen effect on the fatigue behavior of LBM Inconel 718

Simon Puydebois, Abdelali Oudriss, Pierre Bernard, Laurent Briottet, Xavier Feaugas

► **To cite this version:**

Simon Puydebois, Abdelali Oudriss, Pierre Bernard, Laurent Briottet, Xavier Feaugas. Hydrogen effect on the fatigue behavior of LBM Inconel 718. MATEC Web of Conferences, 2018, 165, 10.1051/mateconf/201816502010 . hal-01892915

**HAL Id: hal-01892915**

**<https://hal.science/hal-01892915v1>**

Submitted on 6 Jan 2025

**HAL** is a multi-disciplinary open access archive for the deposit and dissemination of scientific research documents, whether they are published or not. The documents may come from teaching and research institutions in France or abroad, or from public or private research centers.

L'archive ouverte pluridisciplinaire **HAL**, est destinée au dépôt et à la diffusion de documents scientifiques de niveau recherche, publiés ou non, émanant des établissements d'enseignement et de recherche français ou étrangers, des laboratoires publics ou privés.



Distributed under a Creative Commons Attribution 4.0 International License

# Hydrogen effect on the fatigue behavior of LBM Inconel 718

Simon Puydebois<sup>1,2,3</sup>, Abdelali Oudriss<sup>2</sup>, Pierre Bernard<sup>1</sup>, Laurent Briottet<sup>3</sup>, Xavier Feaugas<sup>2</sup>

<sup>1</sup> ArianeGroup, Forêt de Vernon, F-27200, Vernon, France.

<sup>2</sup> LaSIE, CNRS UMR 7356, Université de La Rochelle, F-17000, La Rochelle, France.

<sup>3</sup> Univ. Grenoble Alpes, CEA, LITEN, DTBH, F-38000 Grenoble, France.

**Abstract.** For several years, Inconel 718 made by Laser Beam Melting (LBM) has been used for components of the Ariane propulsion systems manufactured by ArianeGroup. In the aerospace field, many components of space engines are used under hydrogen environment. The risk of hydrogen embrittlement (HE) can be therefore a first order problem. Consequently, to improve the HE sensitivity of LBM Inconel 718, a systematic approach needs to be developed to characterize the microstructure at different scales and its interaction with hydrogen. This study addresses the impact of gaseous hydrogen on the material mechanical behavior under fatigue loadings. In a first step, the low cycle fatigue behavior under 300 bar of hydrogen gas has been evaluated with specimen loaded at a constant load ratio of  $R=0.1$  and a frequency of 0.5 Hz. A reduction in the cycle number of fracture is shown. This reduction of fatigue life is a consequence of the impact of hydrogen damage processes. The impact of hydrogen is evaluated at the stages of crack initiation, crack propagation. These results are discussed in relation with the hydrogen embrittlement mechanisms and particularly in terms of hydrogen / plasticity interactions. To achieve this, the fracture surface morphology was first examined using scanning electron microscopy and second samples near the fracture surface were extracted using Focused-Ion Beam machining from regions containing striation. The main result observed is a reduction of the size of dislocation organization in relation with a decrease of the striation distance.

## 1 Introduction

This study will focus on the fatigue behavior under hydrogen pressure of a material used for the Ariane propulsion systems manufactured by ArianeGroup. This is an Inconel 718 nickel based super alloy made by laser beam melting process (LBM). The additive process (AM) is defined as the process of manufacturing objects by adding material, unlike traditional manufacturing methods such as machining (subtractive fabrication methods). This manufacturing technique has real potential in several industrial fields because of many advantages such as the reduction of the production cycle, more geometrical freedom, precise control of the mass of the parts, reduction of processing steps and flexibility of material selection.

One of the fuels used for propulsion of the upper and lower stages of the Ariane V launcher is hydrogen. Thus, some components are subjected to mechanical loading in a hydrogenated environment.

Since 1950, several studies have shown that hydrogen has a detrimental effect on the mechanical properties of many materials [1-4]. Several studies have been conducted to investigate the impact of hydrogen on Inconel 718 in conventional manufacturing [5-9]. The work of Bruchhausen *et al.* [5] revealed a reduction of the number of cycles to failure when the material is loaded under  $H_2$  pressure. However, no study has been conducted to evaluate the impact of gaseous hydrogen

on the mechanical behavior of Inconel 718 obtained by additive manufacturing method.

The aim of the present work is to evaluate the influence of  $H_2$  on the mechanical properties and on the damage processes of this alloy submitted to low cycle fatigue loading. Firstly, a thorough microstructural analysis has been done to identify the various metallurgical heterogeneities.

Secondly, the mechanical behavior has been studied by low cycle fatigue loading under air and under  $H_2$  gas at room temperature. The impact of hydrogen on the damage process will be discussed with regard to the different stages of damage (crack initiation, crack propagation, toughness). Each of these damage steps has been studied using observations under a scanning electron microscope.

The hydrogen / plasticity interactions during the crack growth process are discussed using samples extracted by Focused-Ion Beam machining from regions containing striation.

## 2 Experimental procedure

The microstructure was investigated at different scales using an optical Leica microscope DM6000M, a Scanning Electron Microscope (SEM Philips FEI Quanta 200FEG / ESEM) associated to an analysis EBSD and a Transmission Electron Microscope (TEM JOEL 2010 200 kV).

\* Corresponding author: [Puydebois.simon@live.fr](mailto:Puydebois.simon@live.fr)

The first step of this metallurgical characterization sought to identify the inclusion state and the presence of porosity. Several studies [10-11] show the presence of porosity inherent to the additive manufacturing process and to the laser parameter (linear laser energy density, laser scanning speed, etc...). The surface preparation consists of mechanical polishing with SiC paper up to grade 4000, followed by OPS polishing on a felted polishing pad. The sample is then rinsed and cleaned in an ultrasonic bath with ethanol, and finally etched for 1 minute 30 seconds in a solution of 1/3 HCL and 2/3 HNO<sub>3</sub>.

In a second step, Electron BackScatter Diffraction (EBSD) helps to identify several metallurgical parameters such as grain size, crystallographic texture, crystallographic grain orientations, grain nature, grain boundary fraction grain and boundary connectivity. The surface preparation prior to EBSD mapping consists of polishing up to grade 4000, diamond paste ¼ µm and vibrating polisher with 0.02µm SiO<sub>2</sub> for 3 hours. The incident electron acceleration voltage is set to 20 kV with a vacuum close to 10<sup>-5</sup> mbar with a measuring step of 3 µm. TSL software analyzes OIM® 5 was used to analyze data from EBSD. These analyses were performed according to two characteristic directions of manufacturing.

The transmission electronic microscope sample is firstly polished with SiC paper up to grade 4000 with a thickness of 80-100µm. This sample is then thinned electrolytically with a Tenupol-5 thinning machine using an electrolyte composed of 450 ml of methanol, 50 ml of perchloric acid and 100 ml of 2-butoxyethanol. The operation is carried out at a temperature around -25°C, under a potential of 10 V [12].

The mechanical properties of low cycle fatigue of Inconel 718 LBM were addressed in air, and under 300 bar of hydrogen at room temperature on axisymmetric fatigue sample. Given that the weakening effect of hydrogen is higher at room temperature [13], the test have been performed at room temperature in order to lead a conservative study. The gage length of each specimen was previously polished with a 4000 grade SiC paper in order to present an identical surface state. Before each fatigue test, four nitrogen rinsing / vacuum cycles are performed followed by a pressure rinsing with the testing gas (hydrogen of high purity 99.9999%) to decrease the level of impurity. These tests were conducted on a hydraulic testing machine equipped with an autoclave. The mechanical load is measured by a load cell located in the pressure chamber. The fatigue tests were carried out with a load ratio of 0.1, for five maximum stress values with a frequency of 0.5 Hz and a triangular signal. After rupture, an observation of the fracture surface was conducted by scanning electron microscopy.

## 3 Results

### 3.1 Microstructural analysis

#### 3.1.1 Inclusion state and porosities

The studied material, Inconel 718 LBM, is mainly composed of 54% Ni, 18% Cr, 17% Fe, 5% Nb and 3% Mo. Following manufacturing, the material was first treated with an annealing treatment to obtain a fine and homogeneous microstructure, then with a second heat treatment to precipitate intermetallic phases ( $\gamma'$  and  $\gamma''$ ).

Energy Dispersive X-ray Spectroscopy analyzes has highlighted the presence of three types of inclusion. The majority of the identified inclusions are aluminas. Titanium carbide and titanium nitride have also been found in smaller proportions. The size of these inclusions varies from 5 to 25 µm. Very few cavities are observed. The area ratio of inclusions and porosities is less than 0.05% of the total surface (fig. 1).

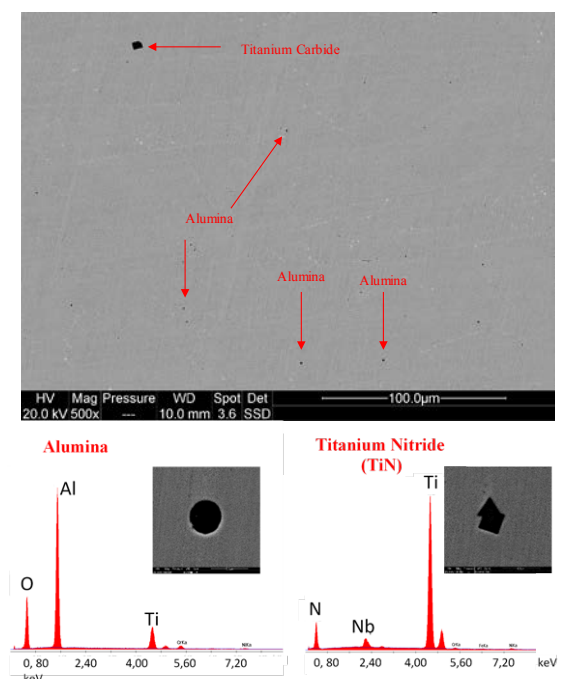


**Fig. 1.** A) SEM observation of porosity and inclusion B) EDS spectrum of alumina C) EDS spectrum of Titanium Nitride

The analysis of the microstructure by optical microscopy after etching and EBSD mapping revealed the grain size homogeneity and a random crystallographic texture in the material whatever the direction. Moreover, EBSD mapping reveals that the majority of the grain boundaries has an index of coincidence  $\Sigma$  below 29 (Fig. 2 B.). A lower scale was observed and identified using TEM, the presence of  $\gamma''$  precipitates in higher proportions and  $\gamma'$  and  $\delta$  in lower proportions was observed. The morphology and size of these precipitates (Fig. 2 C, D, E and F)) has been quantified by TEM analysis.

The Electron BackScatter Diffraction scan shows a random crystallographic texture in the material whatever the manufacturing direction. However, it revealed the heterogeneity of grain size due to the manufacturing process. Figure 3 shows homogeneous grain size distribution along the X and Y axis with a

mean grain size of 62.3  $\mu\text{m}$ . The results along the Z axis show a double grain size distribution with mean values of 66  $\mu\text{m}$  and 153  $\mu\text{m}$ . This is the only observed effect of additive manufacturing on the microstructure of the studied material.

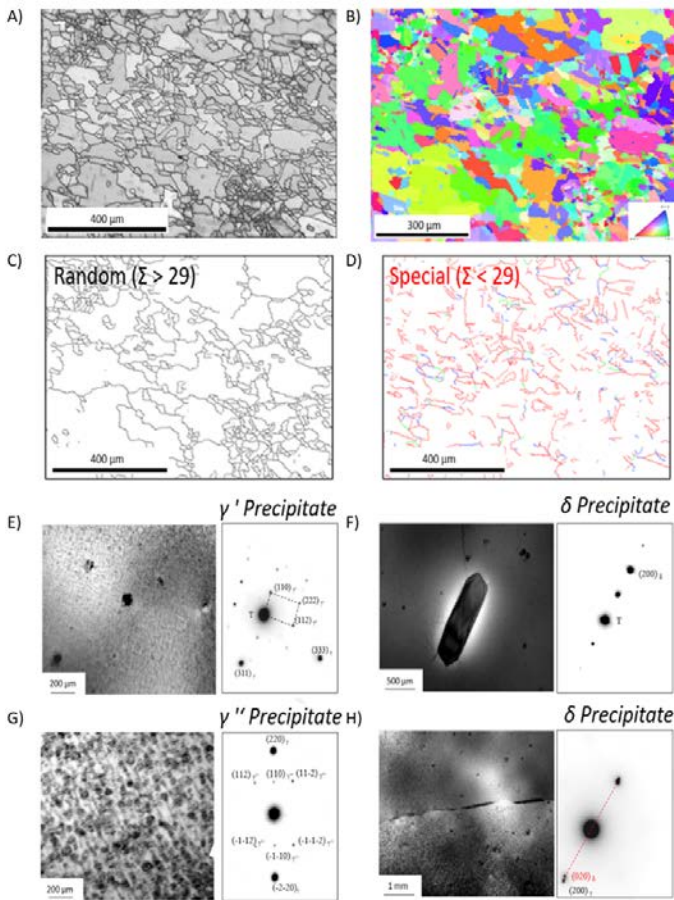


**Fig. 2.** A) EBSD grains mapping along plan 1; B) EBSD orientation mapping; C) EBSD Random grain boundaries mapping D) EBSD Special grain boundaries mapping E) Dark field image and diffraction pattern of the  $\gamma'$  precipitated; F) Dark field image and diffraction pattern of the globular precipitate  $\delta$ ; G) dark field image and diffraction pattern of the  $\gamma''$  precipitated; H) bright field image and diffraction pattern of the acicular precipitate  $\delta$

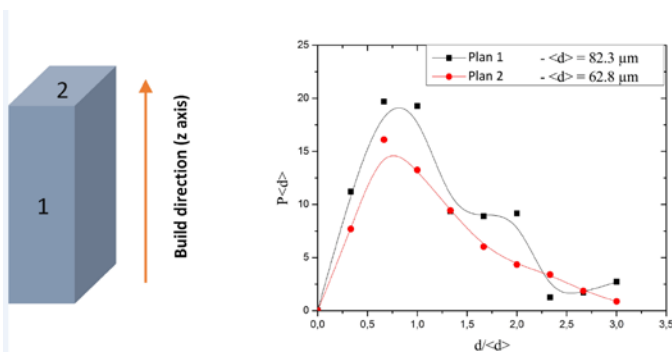


**Fig. 3.** Grain size distribution according to the two normal plans to the additive manufacturing direction

### 3.2 Low cycle fatigue behavior under H<sub>2</sub> pressure

#### 3.2.1 Mechanical results

Figure 4.a shows the S-N curve of Inconel 718 FA displaying the maximum stress versus the number of cycles to failure. First, a decrease is noticed under hydrogen gas compared to samples tested in air. This effect is lower when the stress amplitude is reduced. This reduction in the number of cycles under hydrogen breakdown ranges from a factor 2 for the lowest mechanical loading to a factor of 10 for the highest load.

The fatigue tests were launched after 30 minutes or one day under hydrogen pressure (marked by blue circles). The duration of the immersions before the tests has no effect on the total fatigue life time. The stress/strain fatigue curves shows a fatigue adaptation phenomenon in both conditions illustrated in figure 4.b by a progressive accumulation of plastic strain followed by apparent elastic cycles after stabilization. The stabilization of the plastic strain happens after 10 to 100 cycles of fatigue. The comparison of the two environmental conditions shows that there are no effect of hydrogen on the cumulative plastic strain at stabilization (fig. 4.B).

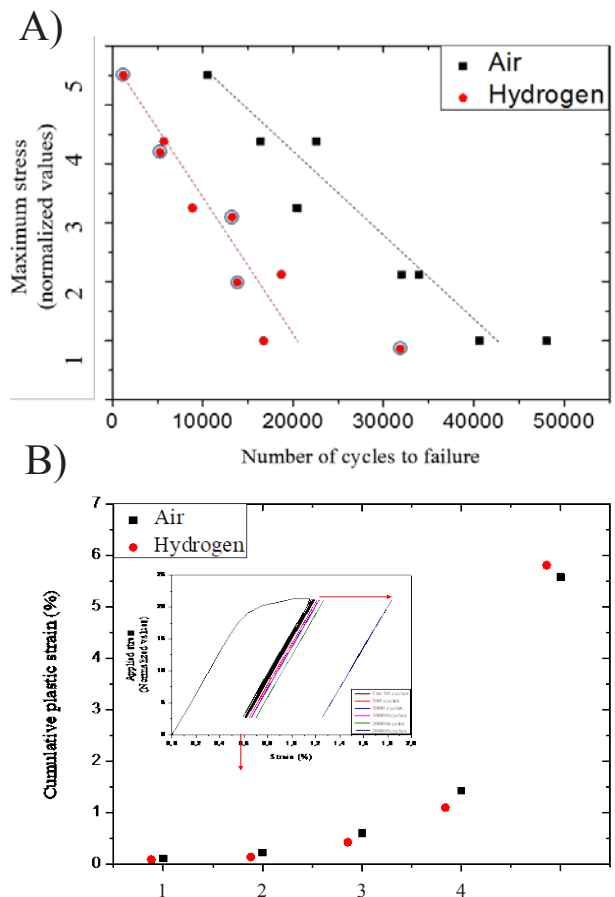


**Fig. 4.** A) S-N curve of Inconel 718 in air and in 300 bar H<sub>2</sub> B) Evolution of the stabilizing plastic deformation as a function of the level of loading for the two experimental conditions (illustration of the adaptation phenomenon)



Figure 4.B shows that hydrogen has no macroscopic effect on the mechanical property of the material. In order to confirm the previous results, observations were made on a smaller scale in the core of the specimen after failure. For each level of stress, we observed the structure of dislocation after failure using a transmission electron microscope.

TEM observations show that under most tested conditions the dislocations structure is organized as a dislocations cell network (table 1). By contrast, the dislocations structure of the higher stress level under hydrogen ( $\sigma_5$ ) presents slip bands. For this experimental condition the number of cycles to failure is low, close to 1000 cycles. In this case, the low density of dislocations did not lead to the formation of dislocations cells. In order to quantify the effect of hydrogen on the dislocation structure, a statistical study of the cells size was performed. For each condition, the average diameter was measured on a sample of 50 dislocation cells.

**Table 1.** Dislocation structure for different stress levels under air and under hydrogen

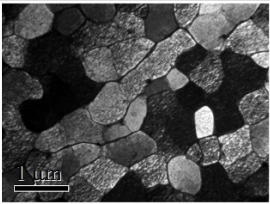
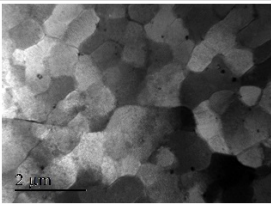
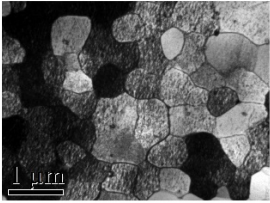
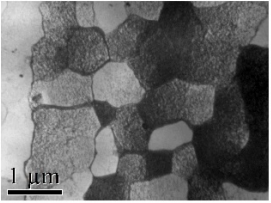
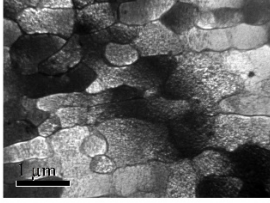
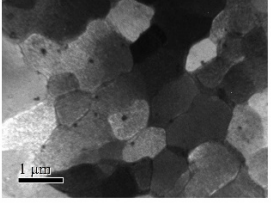
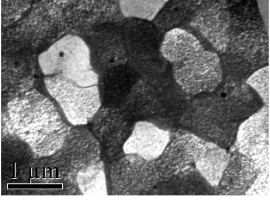
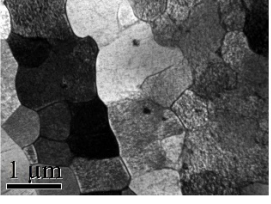
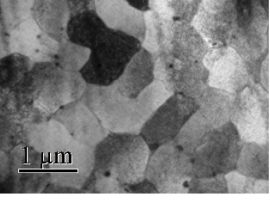
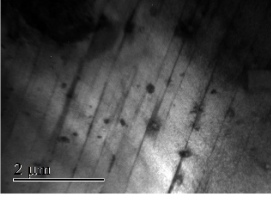
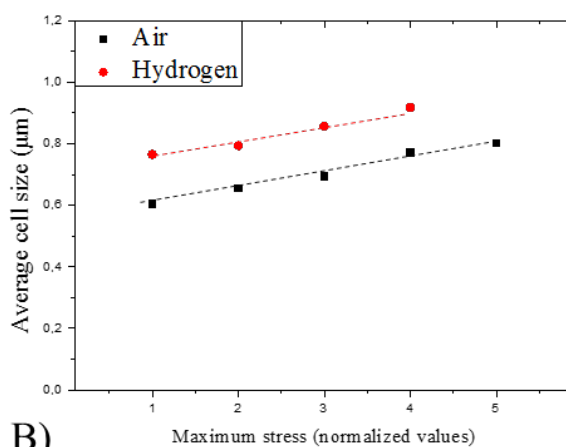
	Air	H
$\sigma_1$		
$\sigma_2$		
$\sigma_3$		
$\sigma_4$		
$\sigma_5$		

Figure 5.a shows a linear evolution of cells size with increasing stress. Moreover, a difference in the mean cells size according to whether the sample was tested under air or under hydrogen is identified. Finally, a relation between the dislocations cells size and the number of cycles to failure is shown (Figure 5.B). This evolution is directly explained by the increase of the dislocation density during cycling. The evolution of the average diameter of dislocation cells is described [14] as proportional to the evolution of the dislocation density:

$$d \approx Kc \cdot \rho_0^{-1/2} \quad (1)$$

with  $Kc$  a constant material,  $d$  the mean diameter of the cells, and  $\rho_0$  the dislocation density.

A)



B)

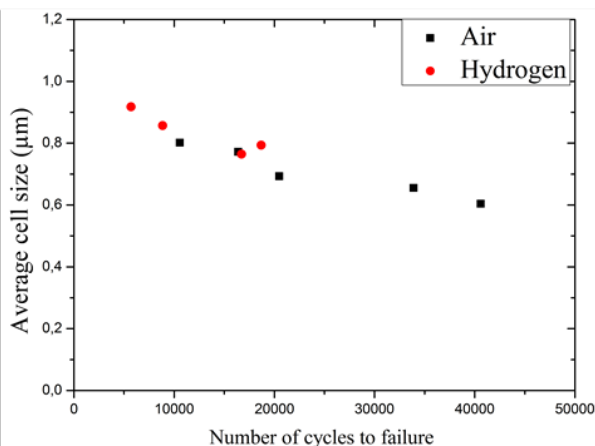


**Fig. 5.** A) Average cell size for different stress levels under both condition B) Average cell size vs. the number of cycles to failure.

The hydrogen effect shown in Figure 5.A is an indirect effect of cell size. Indeed, the evolution of the cell size is not due to the hydrogen/plasticity interaction in the core of the material. This effect is due to decrease of the number of cycles to failure under hydrogen. The low diffusion coefficient of hydrogen in the crystal lattice [15] and in the grain boundary [16] does not allow the hydrogen to reach the center of the specimen after one day under hydrogen. We will therefore question the effect of hydrogen on damage process on the surface.

### 3.2.2 Effect of hydrogen on damage processes

#### 3.2.2.1 Initiation stage

The initiation stage was described in a previous paper [17] using SEM observations. In order to identify the effect of hydrogen on the first step of fatigue life, scanning electron microscope analysis were performed on the gage length surface of the specimen to observe crack initiation.

Under both conditions at failure, the specimen gage length exhibits the emergence of a sliding system, which is present in higher proportion for the tests performed under hydrogen.

Crack initiation takes place on dislocation slip bands under 300 bar of hydrogen (fig.6). The localization of crack initiations under air is not obvious to identify (fig.6).

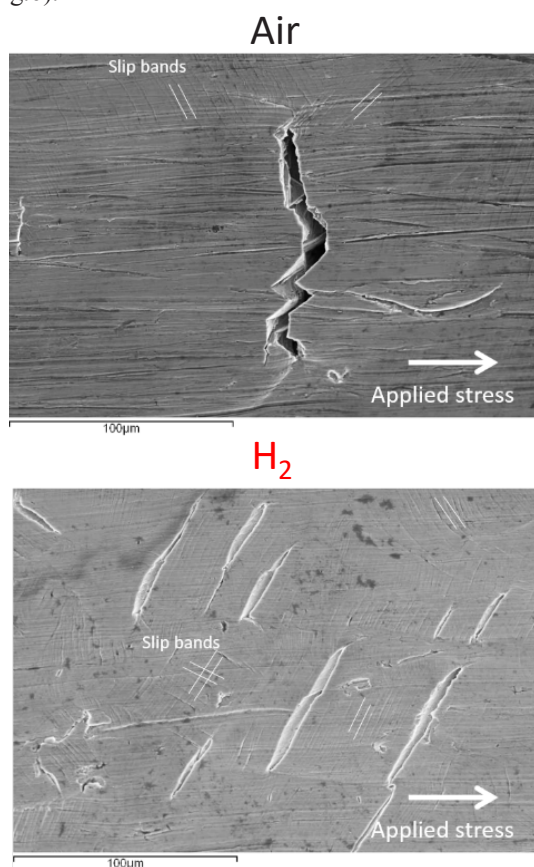


**Fig. 6.** SEM analysis of the gage length of Inconel 718 fatigue specimen in air and in 300 bar H<sub>2</sub> for  $\sigma_2$

For each experimental condition, the density of surface cracks was obtained using 3D optical microscopy along the gage length of the samples.

The results (fig.7) show an increase of the number of cracks with the increasing maximal stress.

Moreover, hydrogen induces an increase in the cracks initiation density by a factor 2 to 8 and a localization of crack initiation close to the fracture surface.

The increase in slip band emergence and crack density under hydrogen is a proof of hydrogen/plasticity interaction with a decrease in cohesion energies at the interfaces (slip system).

Therefore, under hydrogen, crack initiation occurs at lower loads than under air.

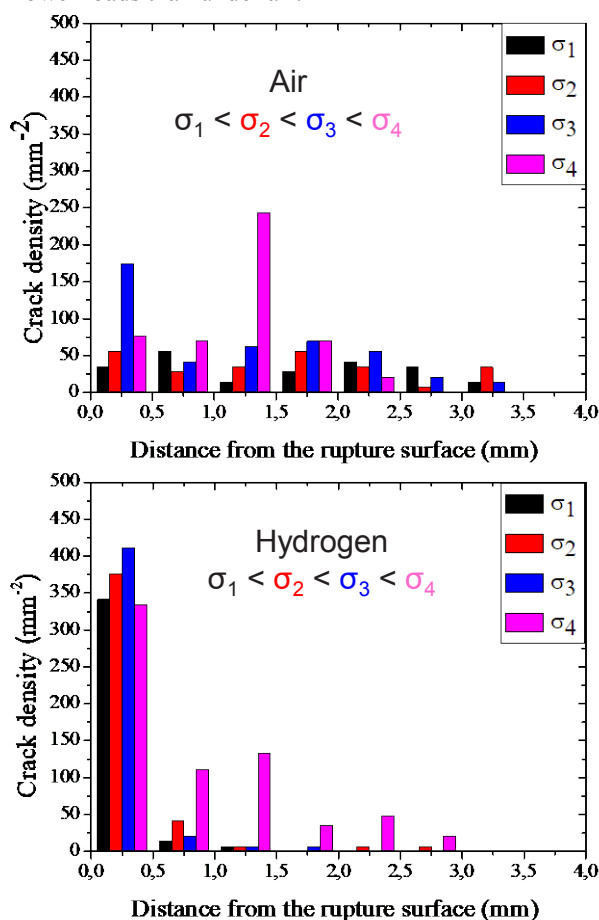


**Fig. 7.** Crack density as a function of the distance from the rupture surface under air and under hydrogen

#### 3.2.2.2 Fatigue crack growth rate (FCGR) determination from LCF tests

In order to quantify the effect of hydrogen on crack growth rate, the following systematic study was carried out. The distance between striations has been measured and reported versus the distance to crack initiation as illustrated in figure 8.

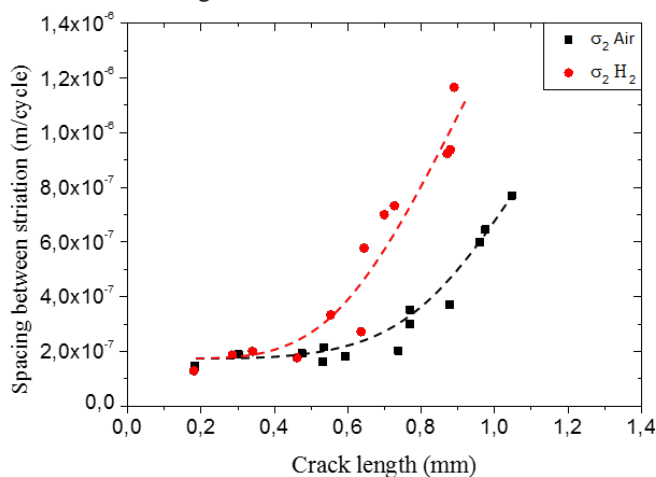


**Fig. 8.** Spacing between striation as a function of the crack length

The correlation between striations and mechanical cycles has been described by many authors as a 1: 1 correlation [18; 19; 20; 21]. Nedbal [22] and Ruckert [23] works respectively on AlCu4Mg1 and Al Alloy 7475-T7351 showed a good correlation between the macroscopic fatigue crack growth rate and the distance between striations for an inter-striation distance ranging between 0.1 and 1  $\mu\text{m}$ .

Considering that one fatigue striation corresponds to one cycle, we can assimilate the distance between striations at the rate of crack propagation. Considering that the tests were performed under stress control, the crack length is directly related to the stress intensity factor

Figure 8 shows the evolution of crack growth rate as function of the crack length for the stress level  $\sigma_2$ . The FCGR is composed of two stages. These two propagation kinetics were also observed by Connors on 7075-T73 aluminum alloy [21].

These results also show an early increase of the crack growth rate in the presence of hydrogen. At this stress level, hydrogen does not appear to have a significant impact on the crack growth rate, for crack lengths lower than 450  $\mu\text{m}$ .

The effect of hydrogen tends to be higher for a higher crack length and hence for a higher stress intensity factor.

### 3.2.2.3 Hydrogen/plasticity interactions during fatigue crack growth

In order to question the impact of hydrogen on the crack growth rate by fatigue striations, thin sections near the fracture surface were extracted using Focused-Ion Beam machining from regions containing striation (fig.9). The purpose of this study is to observe the dislocations structure under the fracture surface at different crack lengths. This study was done for a given stress level  $\sigma_2$ .

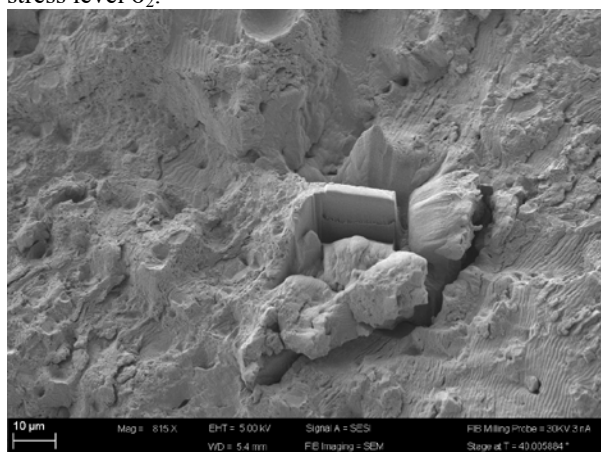


Fig. 9. Illustration of a sampling area ( $a = 1100 \mu\text{m}$  under air)

Sampling was performed at crack initiation (150  $\mu\text{m}$ ), at an intermediate crack length corresponding to the transition of the two kinetics (900  $\mu\text{m}$  under air and 450  $\mu\text{m}$  under hydrogen), and at the crack tip before final rupture (1100  $\mu\text{m}$  under air and 900  $\mu\text{m}$  under hydrogen).

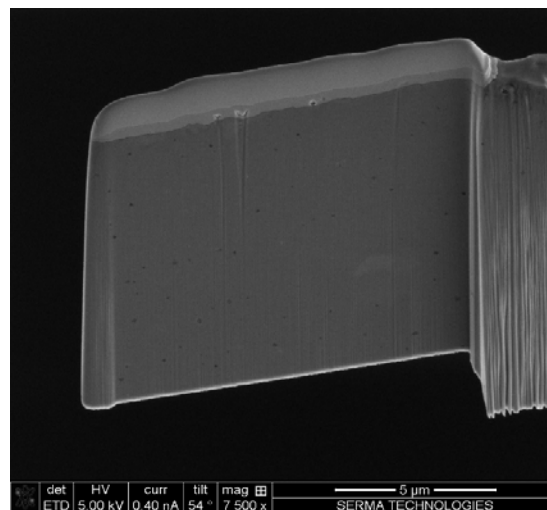


Fig. 10. Example of a FIB thin section ( $a = 900 \mu\text{m}$  under hydrogen)

The first observations show, in all conditions, the presence of slip bands identified by stereographic projection as being on the dense planes of type (111) and in dense directions of type  $\langle 110 \rangle$  (figure 12).

A study of the interband spacing as function of the spacing between striations is presented in Figure 11. The inter-band distance was corrected by a disorientation factor obtained using stereographic projection.

For samples taken after rupture under air, each sliding band is associated with the presence of a fatigue striation. For samples taken under hydrogen, we have a 1: 1 correlation between slip band and fatigue striation for crack lengths lower than 450  $\mu\text{m}$ . Which is highlighted by a  $\cos(45^\circ)$  slope between inter-bands spacing and inter-striations spacing (fig.11).

The sample taken at 900  $\mu\text{m}$  and tested under hydrogen, shows a 1: 1 correlation between fatigue striations and dense primary slip bands (in white line in figure 13). However, on this sample we also observed the presence of micro-bands (in dash line in figure 13). This may reflect an increase in plastic activity in presence of hydrogen.

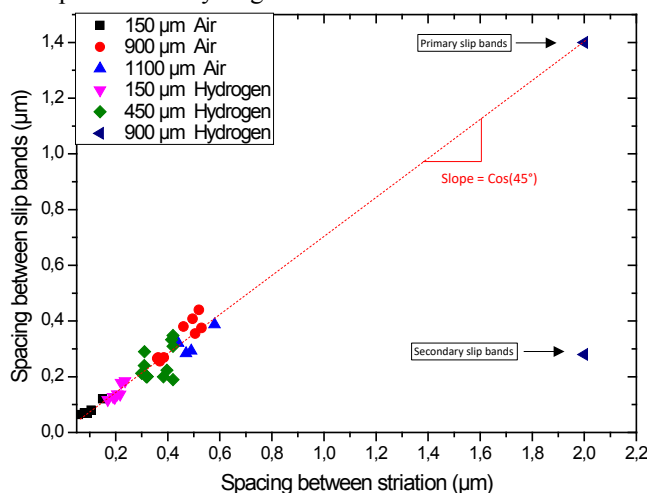
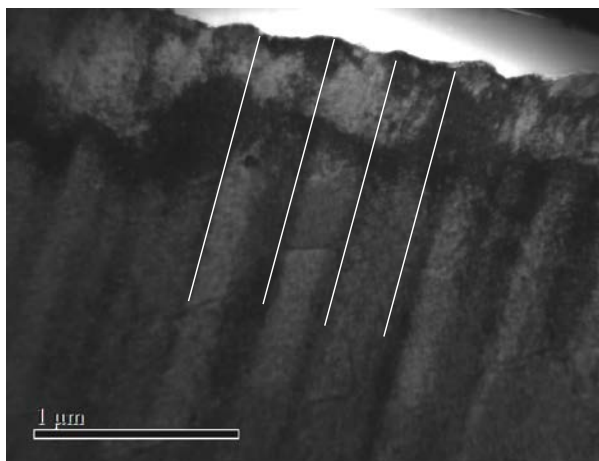
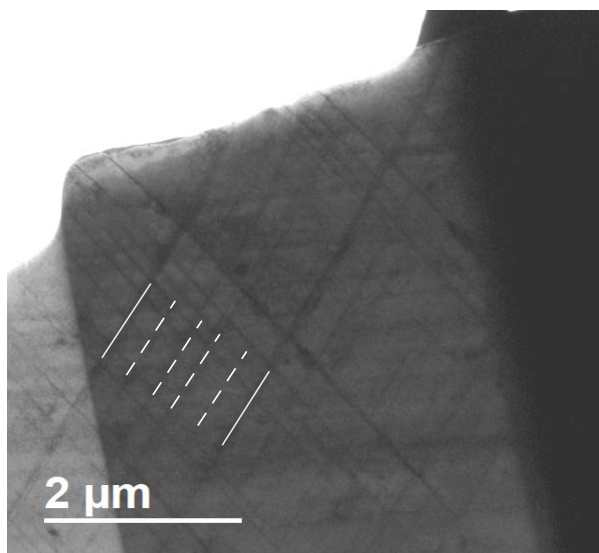


Fig. 11. Spacing between slip bands vs. spacing between striations





**Fig. 12.** TEM observations of the dislocation structure under rupture surface for  $a = 450 \mu\text{m}$  under hydrogen



**Fig. 11.** TEM observations of the dislocation structure under rupture surface for  $a = 900 \mu\text{m}$  under hydrogen

#### 4. Discussion

This study helped to identify the effect of the manufacturing process on the microstructure and the different effects of hydrogen on different stages of low cycle fatigue life. The interactions between hydrogen and microstructure can therefore be questioned:

The low cycle fatigue tests showed a decrease of the lifetime by a factor of 2 to 10. The effect of hydrogen increases with the increasing applied force. It is well known that hydrogen effect on lifetime increases with the increase of stress level and consequently with the plastic activity [24]. The time under hydrogen pressure before test has no effect on the number of cycles to failure. The effect of hydrogen on lifetime seems to be due to the presence of hydrogen on the surface of the specimen during loading.

Indeed, no macroscopic effect of hydrogen has been observed on the cumulated plastic deformation during the study of the ratcheting effect or on the dislocation structure in the tested specimen core. The size of the

cells is directly related to the mechanical history of the material and more precisely to the number of cycles to failure. Hydrogen has no direct effect on the dislocation structure in the test specimen core. Therefore, the study was directed towards the surface phenomena and more precisely the interactions between hydrogen and the mechanism of damage.

SEM observations of gage length show a localization of crack initiation on sliding systems under hydrogen. In addition, an increase in the crack density was observed close to the rupture zone under hydrogen. This location of hydrogen crack density in areas of high plastic activity highlights the presence of interactions between hydrogen and plasticity. The debonding of the sliding system will be facilitated by the presence of hydrogen (HID).

The effect of hydrogen on crack growth rate has also been studied.

The determination of the crack growth rate in low cycle fatigue tests, by the measurement of striation spacing, shows an increase of the crack growth rate under hydrogen pressure.

Focused ion beam (FIB) technique was used to observe the dislocation structure beneath the fracture surface containing striations. These samples were performed to determine how hydrogen impacts the fatigue crack growth.

The observations of samples in air show the presence of sliding bands directly connected to a fatigue striation. This may imply that during each cycle, the activation of a sliding plane allows the blunting of the crack tip and its propagation. We observed the same phenomenon under hydrogen for short crack lengths (lower than  $450 \mu\text{m}$  in this case). For these hydrogen crack length, no effect was observed on the inter-striation spacing and consequently on the crack propagation rate.

For larger crack lengths under hydrogen, we found the presence of sliding macrobands with a 1: 1 correlation with fatigue striation. The observations also show the presence of intermediate bands closer to each other. This secondary network of slip bands has lower dislocations density.

These observations suggest that for higher stress intensity factor under hydrogen a secondary slip network is activated. This can be explained by an increase in plastic activity in presence of hydrogen or/and by an increase in hydrogen/plasticity interactions with the increase in plastic activity.

#### Conclusion

After heat treatment, no effect of additive manufacturing on the microstructure was observed. The only observations that can be associated with additive manufacturing are a bimodal distribution of grain size according to the direction of manufacturing and a small proportion of porosities.

This work has shown a predominant effect of hydrogen/plasticity interaction on the crack initiation step and on the crack growth step. During these two



stages of fatigue, the effect of hydrogen increases with the plastic activity. Hydrogen/plasticity interactions occur only at the material surface.

## Acknowledgements

The authors wish to thank ArianeGroup for their financial support.

## References

1. P. Cotterill; Progr Met Phys (1961), **9**, (4), pp 205–301.
2. H. Johnson, A. Troiano, Nature (1957), **179** (4563)
3. D. Williams, R. J. Jaffee, Less Common Met, (1960), **2** (42)
4. W. Yeniscavich, R. Wolfe, R. Lieberman; J Nucl Mater (1959) ; **1** (3): pp 271–280.
5. M. Bruchhausen, Int. J. Fatigue, (2015), **70** p 137–145
6. J. Jewett, R. Walter, W. Chandler, Frohberg R. NASA contractor report NASA, (1973) **CR-2163**; Rocketdyne;
7. P. Hicks, C. Alstetter, Metall Trans A (1992); **23A**: pp237–249.
8. R. J. Walter and W. T. Chandler, (1973), NASA **CR-124410**
9. V. Frick, G.R. Janser, and J.A. Brown, Space Shuttle Materials (1971), **Vol. 3**, pp. 597- 608
10. J-P. Choi, G-H. Shin, S. Yang, D-Y. Yang, J-S. Lee, M. Brochu, J-H. Yu, Powder Technology (2017), **310**, pp 60–66
11. Q. Jia, D. Gu, Journal of Alloys and Compounds (2014), **585**, pp 713–721
12. L. Xiao, D.L. Chen, M.C. Chaturvedi, Scripta materialia (2005), **52**, pp 603-607
13. V. Frick, G.R. Janser, J.A. Brown, “In: Space Shuttle Materials (1971), **3**, pp.597-608,
14. D. Holt Journal of Applied Phys (1970), **41**
15. J. J.M. Jebaraj, D. J. Morrison, I. I. Suni, Corrosion Science (2014), **80**, pp 517–522
16. T. M. Harris, M. Latanision, Metallurgical Transactions A February 1991, Volume 22, Issue 2, pp 351–355
17. S. Puydebois, A. Oudriss, L. Briottet, X. Feugas, P. Bernard, International Hydrogen Conference (2016) Jackson Lake (USA) pp 324-331
18. J. Au, J. S. Ke, ASTM STP733 (1980), p. 202
19. P.J.E. Forsyth and D. A. Ryder, ACTA Metallurgica (1961), **63**, pp 117-124
20. L. De Baglion de La Dufferie, Manuscript for PhD Ecole Nationale Supérieure de Mécanique et d’Aérotechnique de Poitiers, 2011.
21. W.C. Connors, Mater. Charact (1994). **33** (3) pp 245–253.
22. I. Nedbal, J. Siegl, J. Kunz, Advances Fracture Research (Proc. ICF 7). Eds. K. Salama et al. Vol. **5**. Oxford, Pergamon Press (1989), p. 3483-3491.
23. C.O.F.T. Ruckert, A.A. Messias Filho, W.W. Bose Filho, D. Spinelli, and J.R. Tarpani, Journal of Materials Engineering and Performance (2011), **20** (3), pp 381-389
24. J. A. Harris, M.C. VanWanderham, (1973). Final Report to NAS8-26191, Pratt and Whitney Government Products Division.